Effects of the Introduction of L-Nucleotides into DNA. Solution Structure of the Heterochiral Duplex d(G-C-G-(L)T-G-C-G)·d(C-G-C-A-C-G-C) Studied by NMR Spectroscopy[†]

M. J. J. Blommers,[*,‡] L. Tondelli,[§] and A. Garbesi[§]

Department of Physics, Ciba-Geigy A.G., CH-4002 Basel, Switzerland, and ICoCEA–CNR, via P. Gobetti, 101, 40129, Bologna, Italy

Received December 27, 1993; Revised Manuscript Received April 5, 1994[®]

ABSTRACT: The effect of the substitution of a L-nucleoside for a D-nucleoside in the duplex d(G-C-G-T-G-C-G)·d(C-G-C-A-C-G-C) was studied by UV and NMR spectroscopy. These unnatural oligonucleotides have potential for antisense DNA technology [Damha, M. J., Giannaris, P. A., & Marfey, P. (1994) *Biochemistry* (preceding paper in this issue)]. The thermal stability of such duplexes is lower than that of the natural one and is dependent on the nucleotide type and/or sequence. Interestingly, inversion of the chirality of thymidine but not adenosine coincides with a large stabilizing enthalpy change. The structure of the heterochiral duplex d(G_1-C_2-G_3-(L)T_4-G_5-C_6-G_7)·d(C_8-G_9-C_{10}-A_{11}-C_{12}-G_{13}-C_{14}), where (L)T denotes the mirror image of the natural thymidine, has been determined by NMR spectroscopy. The sugar conformation was determined using the sum of coupling constants and the distances using a model free relaxation matrix approach. The torsion angles of the backbone follow from $^3J_{HH}$, $^3J_{HP}$, and $^4J_{HP}$ coupling constants. The structure of the duplex was calculated by metric matrix distance geometry followed by simulated annealing. The structure is close to that of B-DNA. The base pair formed by (L)T and A is of the Watson–Crick type. All sugars adopt an S-type pucker. The incorporation of the L-sugar in the duplex is accomplished by changes in the backbone torsion angles around the phosphates and the glycosidic torsion angle of (L)T. The modification induces changes in the natural strand as well. The structure exhibits an unusual interaction between the aromatic rings of the (L)T_4·A_{11} and G_3·C_{12} base pairs, which provides a plausible explanation of the unusual thermodynamic properties of the duplex.

The use of oligonucleotides to inhibit specifically the expression of a given gene has become a very active research area (Editors, 1993), endowed with potential therapeutic application (Uhlmann & Peyman, 1990; Milligan et al., 1993). The rationale of this strategy (Hélène & Toulme, 1990; Thuong & Hélène, 1993) is based upon the binding of a synthetic oligonucleotide to a segment of the target nucleic acid in a sequence-specific mode, dictated by the Watson–Crick (anti-messenger approach) or Hoogsteen (anti-gene approach) base-pairing scheme. One of the many hurdles facing the effective implementation of this principle is the fast and extensive degradation of natural oligonucleotides by nucleases. To overcome this and related problems, like penetration through the cell membrane, many strategies have been pursued (Uhlmann & Peyman, 1990; Morvan et al., 1993) to modify the chemical structure of oligonucleotides, with special attention being paid to the internucleosidic backbone. Several promising analogues have been found, inter alia phosphorothioates (Uhlmann & Peyman, 1990; Yaswen et al., 1993), phosphorodithioates (Marshall & Caruthers, 1993), methyl phosphonates (Uhlmann & Peyman, 1990), and peptide nucleic acids (Egholm et al., 1993). Inversion of the configuration of the anomeric carbon of the sugar moiety has led to α-oligonucleotides (Imbach et al., 1989), which have good stability in biological media and bind rather efficiently to the target sequence.

Along the line of changing the stereochemistry of the chiral centers present in natural nucleic acids, we have recently studied the behavior of L-2'-deoxyoligonucleotides (L-DNA),[1] whose resistance to nucleolytic enzymes is well documented (Asseline et al., 1991), where the natural D-sugar is replaced by the L-enantiomer. Unfortunately, medium-length L-DNAs, containing all four natural bases in a random distribution, fail to anneal to complementary, single-stranded DNA and RNA in both antiparallel and parallel orientations (Garbesi et al., 1993). To explore other possible applications of L-nucleosides in the field of antisense oligonucleotides, we (Capobianco et al., 1991) and others (Damha et al., 1991) have already directed attention to mixed L/D-DNA oligomers and have found that L-2'-deoxynucleosides at the terminal positions of a natural oligomer enhance significantly its stability toward exonuclease digestion (Damha et al., 1991), leading to a higher biological activity than that of the corresponding unmodified sequence (Capobianco et al., 1991). Since it was foreseeable that some L-residues "scattered" through a natural sequence in a heterochiral oligonucleotide could enhance its resistance toward endonucleases as well, it seemed worthwhile to compare the thermodynamic stability and structural features of a natural DNA duplex with those of modified analogues, where one of the internal nucleosides was replaced by its L-enantiomer. While this research was in progress, we were informed by Masad Damha [personal communication; see

[1] Abbreviations: NMR, nuclear magnetic resonance; NOE, nuclear Overhauser enhancement; TOCSY, total correlation spectroscopy; COSY, correlated spectroscopy; DQF-COSY, double quantum filtered COSY; HMQC, heteronuclear multiple quantum correlation; UV, ultraviolet; DNA, deoxyribonucleic acid; C, cytosine; T, thymine; G, guanine; A, adenine; D-DNA, natural DNA with D-deoxyriboses; L-DNA, mirror image of natural DNA with L-deoxyriboses.

also Damha et al. (1994)] that mixed L/D-2'-deoxyoligo-nucleotides bind complementary single-stranded DNA and RNA, giving duplexes whose thermal stabilities are for some cases comparable with the requirement of the antisense methodology.

Our interest in the detailed knowledge of the structure of heterochiral DNA duplexes was also connected to ongoing research on the mechanism of the antiproliferative activity of L-thymidine against HSV-1 (Spadari et al., 1992). Preliminary results (G. Maga, private communication) show that, in the presence of natural templates, different cellular and viral DNA polymerases accept as a substrate L-TTP, leading in some cases to incorporation of L-thymidine into the growing chain.

In a more general perspective, chimeric DNA and RNA molecules, where one or more D-sugars are replaced by their L-enantiomers, i.e., heterochiral oligonucleotides, are a new class of nucleic acids, whose structure, most likely yet another variation on the standard A- or B-type helix, should add to our insight into the basics of nucleic acid polymorphism. In the present study, DNA duplexes I–IV were characterized by UV and NMR spectroscopy:

d(G-C-G-T-G-C-G)·d(C-G-C-A-C-G-C)   (I)

d(G-C-G-(L)T-G-C-G)·d(C-G-C-A-C-G-C)   (II)

d(G-C-G-T-G-C-G)·d(C-G-C-(L)A-C-G-C)   (III)

d(G-C-G-(L)T-G-C-G)·d(C-G-C-(L)A-C-G-C)   (IV)
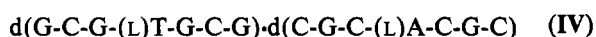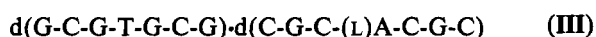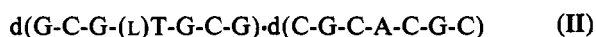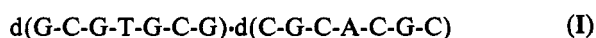
(L)T and (L)A indicate L-thymidine and L-adenosine, respectively. All modified duplexes II–IV are destabilized with respect to I. Surprisingly, the replacement of a D-thymidine by L-thymidine (duplex II) results in a large, stabilizing enthalpy change, which is accompanied, however, by a dominant entropic penalty. This finding is nicely accounted for by the geometrical features of the central core of duplex II, whose structure determination by NMR spectroscopy is the main object of the present work.

MATERIALS AND METHODS

Oligonucleotide Synthesis. The oligodeoxynucleotides were synthesized using the standard β-cyanoethylphosphoramidite methodology with a Pharmacia DNA automatic synthesizer (10-μmol scale). The natural D-phosphoramidite reagents and the derivatized supports were from Pharmacia. L-Phosphoramidites were prepared and characterized as previously described (Garbesi et al., 1993). After deprotection with NH$_4$OH, the crude oligomers were purified by anion-exchange chromatography on DEAE-Sephacell (Pharmacia) using a linear gradient from 0.05 to 1.0 M triethylammonium bicarbonate (pH = 7.4). Fractions were analyzed by HPLC, and those having a titer > 95% were collected, coevaporated with water several times to remove the buffer, and converted to the sodium salt with Dowex 50 W × 8. The final purity was at least 97% for each oligomer (reversed-phase HPLC: Spherisorb RP18, 5 μm, 25 cm × 0.46 i.d., T = 30 °C, 1 mL/min, CH$_3$CN gradient in 0.05 M KH$_2$PO$_4$, pH 4.5).

UV Melting Experiments and Thermodynamic Parameters. UV melting experiments were carried out on a Varian Cary/ 3E UV–visible spectrophotometer equipped with a Cary temperature controller. The cell compartment was equilibrated with a flow of nitrogen at temperatures below 30 °C. Annealing was performed by heating the sample at 80 °C and gradually cooling it to –3 °C. Then, the temperature was increased in steps of 0.5 °C/min, and the UV absorbance was

measured at 260 nm. The collected data points were fitted on the basis of a nonlinear least squares refinement procedure (Freier et al., 1986) on the assumption of an all-or-none melting process (Gralla & Crothers, 1973).

NMR Experiments. Samples (3.3 mM) of duplexes I, II, and III were prepared in an 80 mM phosphate buffer, pH 6.0, with 200 mM NaCl. 1D experiments and 1D-NOE experiments on the samples in 95% H$_2$O/5% D$_2$O were recorded at 400 MHz on a Bruker AM400 spectrometer interfaced with an Aspect3000 computer using a time-shared long pulse. After data collection, the free induction decays were treated with digital shift addition (Hilbers & Haasnoot, 1983). Then, the first two points of the time domain spectra were calculated using linear prediction (Barkhuijsen et al., 1985). On the same instrument a proton-detected ^{1}H–^{31}P HMQC experiment without decoupling of ^{31}P during acquisition was recorded as described before (Blommers et al., 1991) using an inverse ^{1}H broad-band probe head. A proton-detected ^{1}H–^{13}C HMQC experiment without decoupling of ^{13}C was recorded on a Bruker AMX 600 spectrometer.

All homonuclear 2D experiments of the samples in D$_2$O were recorded on a Varian U500 spectrometer operating at a frequency of 500 MHz. NOESY experiments (Jeener et al., 1980) were recorded with mixing times of 200–500 ms. Clean-TOCSY experiments (Braunschweiler et al., 1983; Griesinger et al., 1988) were recorded with mixing times of 20–120 ms. All 2D experiments were recorded at 25 °C. These phase-sensitive 2D spectra were recorded with 400 experiments and 2048 complex data points using quadrature detection in both dimensions (States et al., 1982). A DQF-COSY experiment (Piantini et al., 1982) was recorded with 600 experiments and 4096 complex data points.

Data were transferred to a Silicon Graphics workstation and processed using the software package FELIX 2.05 (BIOSYM). The 2D data sets were apodised using shifted sine bell or Gausian filters and zero-filled to 1024 data points in the t_1 dimension.

Structure Elucidation. Structure calculations were carried out in the following order. First the sugar conformation was examined using the sums of the coupling constants $\Sigma \ 1' = J_{1'2'} + J_{1'2''}$, $\Sigma \ 2' = J_{1'2'} + J_{2'2''} + J_{2'3'}$, and $\Sigma \ 2'' = J_{1'2''} + J_{2'2''} + J_{2''3'}$ measured from the DQF-COSY spectrum. The experimental values were evaluated using the program MARC (Blommers et al., 1991) assuming an error of 1 Hz in the determination of the sums of the coupling constants. The program finds all combinations of S-type and N-type sugars as well as their molar fraction, which can be described by the above mentioned experimental data within the error limit.

Then, the glycosidic torsion angle of each mononucleotide unit was estimated using the integrated NOE intensities of the NOESY spectrum recorded with a mixing time of 200 ms in combination with simulated NOESY intensities using the program NOESIM (Keepers & James, 1984; Blommers et al., 1987). A rotational correlation time of 1.5 ns was used. This value was calculated using the Stokes–Einstein equation as described before (Blommers et al., 1991).

Subsequently, the distances between the residues in the DNA duplex were estimated using the program NOEFIT. This program fits the relaxation matrix in a procedure where the interresidue NOEs are fitted in the order of their individual intensities (Blommers et al., 1991; van de Ven et al., 1991).

Distance geometry calculations were carried out using the program DGII (Havel, 1991) which is integrated into the molecular modeling package InsightII (BIOSYM) running on a Silicon Graphics 4D/300 GTX. Upper and lower bound
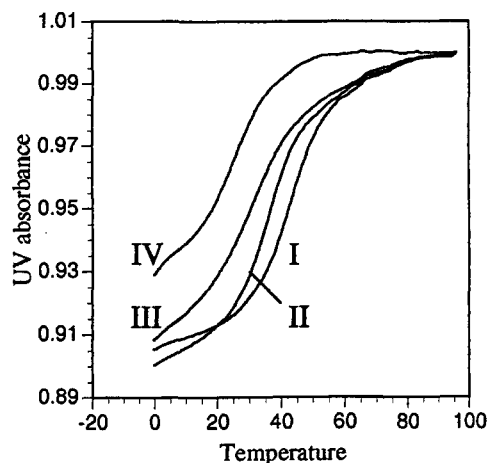
FIGURE 1: UV melting profiles (260 nm) obtained for duplexes I–IV at 8 μM concentration. The curves are scaled such that the UV absorbances are equal at high temperature, i.e., when the oligo-nucleotides are single stranded. The temperature is indicated in °C.

distances were smoothed using triangle smoothing as well as tetrangle smoothing for sequential residues. For all residues, apart from distance and dihedral restraints, chiral restraints were added. These chiral restraints (treated as so-called volume restraints) ensure the proper chirality of each chiral center. Thus, for the L-residue, a L-deoxyribose was obtained. The structures were embedded and optimized using a four-dimensional Cartesian space. The embedded structures were further refined using 10 000 steps of simulated annealing.

Distance geometry structures were further studied using energy minimization and subsequent molecular dynamics calculations using the AMBER force field (Weiner et al., 1986). The electrostatic interactions were scaled to $1/4r_{ij}$. This scaling approximates the distance-dependent dielectric function proposed by Lavery et al. (Fritsch & Westhof, 1990). The calculation was carried out with a step size of 1 fs. The temperature was 300 K. The equilibration was done in 1 ps; then the simulation was carried out for 100 ps.

RESULTS

UV Melting Experiments. The duplexes I–IV were prepared by mixing the complementary sequences 1:1. The thermodynamic stabilities of the duplexes were subsequently studied by UV melting experiments. The corresponding melting curves are shown in Figure 1. All mixtures give rise to the formation of a duplex, which melts out, at 8 μM single-strand concentration, between 26 and 40 °C (cf. Table 1). Cooperativity of melting is preserved in all cases. The thermodynamic parameters were calculated from the UV melting curves as described in Materials and Methods. As far as the melting temperature is concerned, the natural sequence (I) is the most stable. Surprisingly, the substitution of one D-unit by a L-unit has different effects on the stability (duplexes II and III). Thus, the thermodynamic properties depend on the place of the L-nucleoside in the sequence and/or on the type of nucleoside (cf. Table 1, Figure 1). Two opposite, substituted
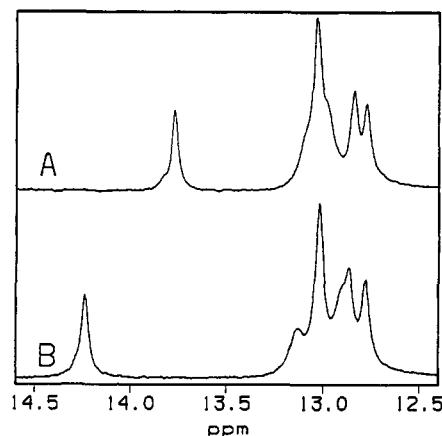

FIGURE 2: Imino proton spectra of duplexes I (A) and II (B) recorded at 5 °C. The low-field signal corresponds to the D- or L-thymidine imino proton.

L-nucleosides (duplex IV) cooperate to produce the destabilization effect observed for duplexes II and III. Further inspection of the melting curve of duplex IV shows a second transition at low temperature. This transition is concentration independent. At low temperature the oligonucleotide d(G-C-G-(L)T-G-C-G) forms an unusually stable mini-hairpin structure, as confirmed by other NMR experiments (data not shown). The change in enthalpy upon melting of duplex II is substantially higher than in any of the other duplexes, including the natural one ($\Delta\Delta H = 14$ kcal). This intriguing effect on the thermodynamic parameters in the case of II prompted us into a more elaborate study of this modified duplex by NMR spectroscopy.

NMR Experiments. (A) Imino Proton Spectra. Duplexes I, II, and III were studied with 1D NMR. The corresponding imino proton spectra of I and II are shown in Figure 2. The imino proton of thymidine in the natural duplex resonates at 13.8 ppm, downfield from the G imino proton resonances, as expected.

1D NOE difference experiments without presaturation of the solvent were performed (see Materials and Methods). Irradiation of the low-field signal results in a strong NOE (10.0%) on the adenosine H2 resonance at 7.70 ppm. The imino proton NMR spectrum of the unnatural duplex II resembles that of the natural duplex with the exception of the low-field signal, which shifted to 14.25 ppm. Again, a 1D NOE experiment, where the low-field signal is irradiated, results in a strong NOE (11.5%) at an aromatic proton resonance at 7.88 ppm, establishing the assignment of the low-field signal to the imino proton of the L-thymidine. These experiments show that in II a base pair is formed between the modified thymidine and the adenosine in the complementary strand. The type of base pair, however, cannot be established from such experiments.

The imino proton spectra of both duplexes were studied as a function of the temperature. The melting of the duplexes was observed by a broadening of all imino proton signals. The

Table 1: Thermodynamic Parameters Obtained by UV Melting Experiments[a]

duplex	ΔH (kcal/mol)	ΔS [cal/(mol K)]	T_m (°C)
I d(G-C-G-T-G-C-G)·d(C-G-C-A-C-G-C)	52	143	40
II d(G-C-G-(L)T-G-C-G)·d(C-G-C-A-C-G-C)	66	191	35
III d(G-C-G-T-G-C-G)·d(C-G-C-(L)A-C-G-C)	49	138	31
IV d(G-C-G-(L)T-G-C-G)·d(C-G-C-(L)A-C-G-C)	59	173	26

[a] The four duplexes differ on the basis of the chirality of the central nucleotide of one of the strands. (L)T and (L)A are mirror image nucleotides containing L-deoxyribose. The other nucleotides (when not indicated) are natural ones.
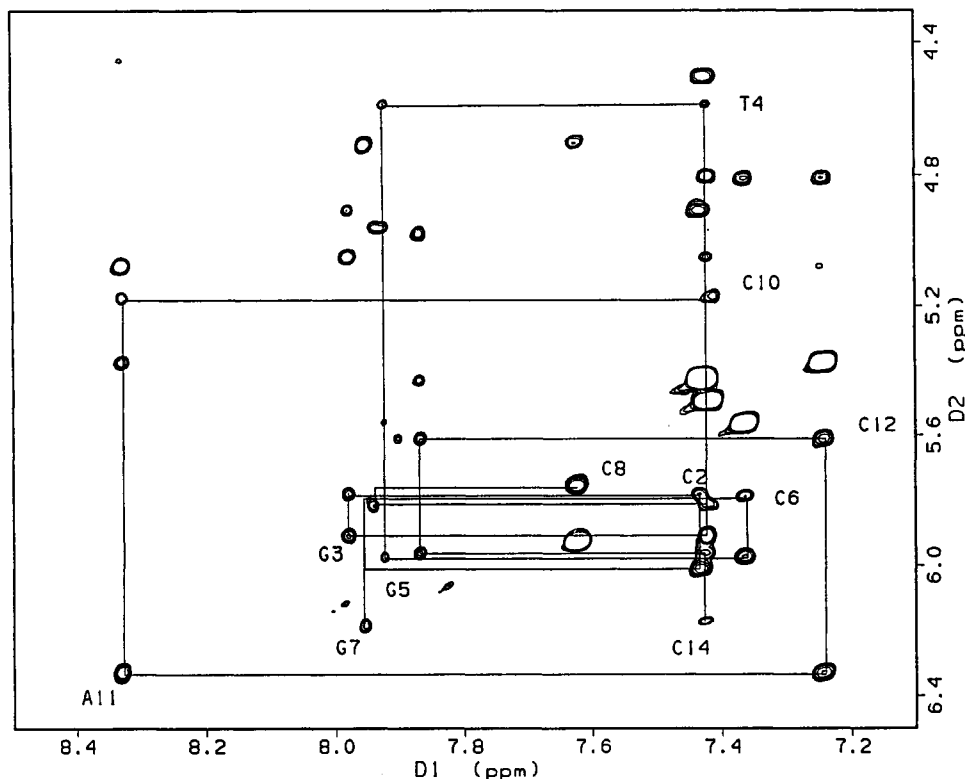
FIGURE 3: Part of the NOESY spectrum of duplex II, recorded with a mixing time of 400 ms and a temperature of 23 °C. The sequential cross peaks between the aromatic proton resonances and the sugar H1′ resonances are connected by lines. The labels indicate the intraresidue cross peaks.

L-thymidine imino proton resonance vanishes from the spectrum around 43 °C at the same temperature as the guanine imino protons. The line widths of (L)T and (D)T in both duplexes were comparable in all spectra, indicating that the melting of the unnatural (L)T·A base pair occurs cooperatively with that of the other base pairs in the duplex.

Similar experiments were performed for duplex III. The NH proton of (D)T resonates at 13.95 ppm, and irradiation of this resonance results in a NOE of 4% at 7.6 ppm, which confirms the presence of a base pair between (L)A and (D)T. At room temperature the line width of the NH proton resonance of (D)T is significantly broader than the other NH resonances.

Duplex II formed between the oligonucleotides D-d(G-C-G-(L)T-C-G-C) and D-d(C-G-C-A-C-G-C) was subsequently investigated by 2D NMR.

(B) Resonance Assignment. The ^{1}H spectrum was assigned on the basis of homonuclear 2D experiments using standard methods (Haasnoot et al., 1983; Hare et al., 1983). To this end, NOESY experiments with different mixing times, TOCSY experiments, and a DQF-COSY experiment were recorded. The residues are numbered as in $(5'\rightarrow3')$D-d(G$_1$-C$_2$-G$_3$-(L)T$_4$-G$_5$-C$_6$-G$_7$)·$(5'\rightarrow3')$D-d(C$_8$-G$_9$-C$_{10}$-A$_{11}$-C$_{12}$-G$_{13}$-C$_{14}$). One part of the NOESY spectrum recorded for a mixing time of 400 ms is shown in Figure 3. It shows connectivities between the aromatic proton resonances and the sugar H1′ resonances. The sequential assignment can readily be made by connecting all neighboring residues of the natural strand, i.e., residues 8–14. Most of the NOEs involving H6/H8 and H1′ protons within a residue are labeled with the residue name and number. Note that the C$_{10}$H1′ resonance is shifted upfield to 5.2 ppm. The sequential assignment can also be done in the H6/8–H2′/2″ region of the spectrum and is consistent with the cross peaks found for the 1′–2′ and 1′–2″ pairs in the NOESY, TOCSY, and DQF-COSY spectra. Apart from

Table 2: Assignments of the ^{1}H Resonances of the Duplex II Formed by d(G$_1$-C$_2$-G$_3$-(L)T$_4$-G$_5$-C$_6$-G$_7$) and d(C$_8$-G$_9$-C$_{10}$-A$_{11}$-C$_{12}$-G$_{13}$-C$_{14}$) at 25 °C^a

	H8 H6	H5 H2 CH3	H1′	H2′	H2″	H3′	H4′	H5′	H5″
G1	7.93		5.97	2.60	2.78	4.85	4.12	3.72	4.25
C2	7.40	5.42	5.75	2.12	2.45	4.88	4.19	4.13	4.13
G3	7.95		5.87	2.62	2.69	5.02	4.34	4.04	4.12
T4	7.40	1.45	4.70	1.74	2.41	4.78	4.56	4.14	4.18
G5	7.90		5.94	2.58	2.71	4.95	4.37	4.06	4.06
C6	7.34	5.53	5.74	1.87	2.32	4.67	4.18	4.07	4.07
G7	7.92		6.15	2.62	2.38	4.68	4.18	4.06	4.06
C8	7.59	5.88	5.71	1.88	2.32	4.67	4.18	4.07	4.07
G9	7.91		5.78	2.62	2.62	4.97	4.31	3.94	4.05
C10	7.41	5.46	5.12	1.98	2.11	4.79	4.10	4.10	4.10
A11	8.30	7.88	6.31	2.90	2.90	5.05	4.43	4.10	3.96
C12	7.22	5.34	5.57	1.88	2.27	4.78	4.13	4.13	4.13
G13	7.78		5.93	2.57	2.69	4.95	4.37	4.06	4.06
C14	7.36	5.32	6.12	2.19	2.19	4.47	4.02	4.24	4.24

^{a} The chemical shifts are given relative to DSS. All of the H2′ and H2″ and some of the resolved H5′ and H5″ protons are assigned stereospecifically using a qualitative interpretation of J-couplings and NOE intensities (see text).

the unusual shift of the C$_{10}$H1′ resonance, the contacts and chemical shifts are in accordance with a regular helix. A more elaborate analysis is described in the next section. The resonance assignment of the other sugar protons was achieved using the TOCSY experiments recorded at longer mixing times, e.g., 120 ms, in combination with the NOESY spectrum. The results are given in Table 2.

The sequential assignment in the other strand is more complicated than that described above, since no assumptions can be made as to the structure around the L-nucleoside and the type of base pair formed between (L)T and (D)A. The assignment started with a collection of all possible trivial contacts. The two unassigned cytosine H5–H6 cross peaks in NOESY and DQF-COSY were identified, as well as possible H5(n)–H1′(n − 1) contacts in the NOESY spectrum. The
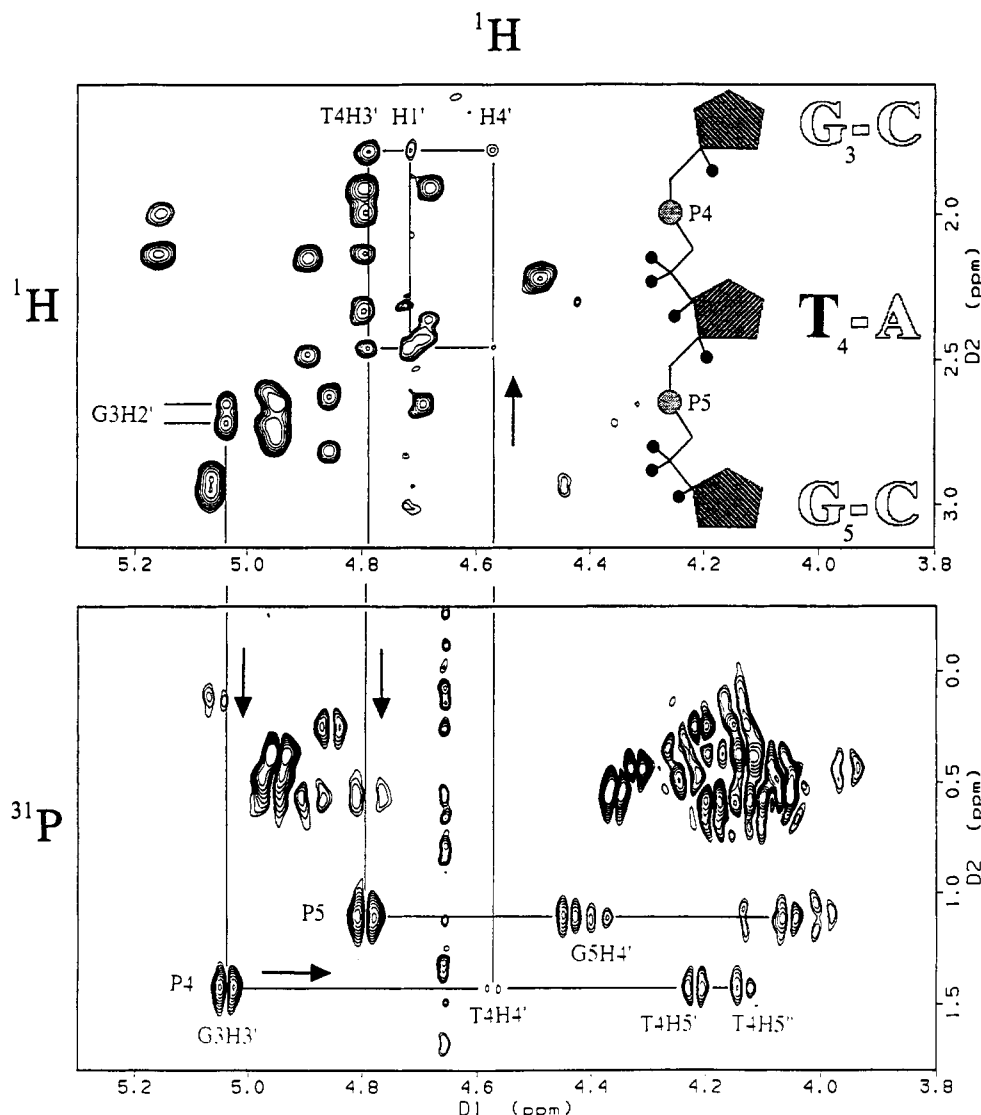
^{1}H

FIGURE 4: Part of the NOESY spectrum of duplex II, recorded with a mixing time of 200 ms (top), and the corresponding ^{1}H–^{31}P HMQC spectrum (bottom). The sequential assignment of the backbone resonances in the G$_3$-(L)T$_4$-G$_5$ part of the duplex (top, inset) is indicated.

CH$_3$–H6 cross peak of (L)T could be identified in the NOESY and TOCSY experiments. Also a NOE cross peak between the (L)T$_4$ methyl proton resonance and an aromatic resonance, possibly H8 of G$_3$ or G$_5$, was observed. Initially, discrimination between the latter aromatic resonances was not straightforward since the aromatic protons of T$_4$, C$_2$, and C$_{10}$ overlap, and therefore one could not assign all cross peaks unambiguously at that stage. However, after most of the contacts were collected, preliminary distance geometry calculations were carried out. These calculations showed that only one assignment is consistent with all NOE data observed thus far. The assignment was further complicated because the H1' resonance of (L)T$_4$ could not be located in the region were H1' protons normally resonate. Although cross peaks between the H2' and H2'' resonances of (L)T$_4$ and one H1' resonance were identified, the corresponding cross peaks were absent in the DQF-COSY and TOCSY experiments. These cross peaks should therefore be interpreted as interresidue contacts between the L-sugar proton and the neighboring sugar proton. It was then discovered that the (L)T$_4$H1' resonates at 4.6 ppm, which is a position shifted about 1.2 ppm upfield relative to that normally found for thymidine H1' (Van de Ven & Hilbers, 1988b). The assignment of this unusual chemical shift is corroborated by the observation of an H1'–H2' cross peak in the DQF-COSY experiment and cannot be mistaken

for an H3' resonance. H2'–H3' cross peaks are also observed. In addition, a ^{1}H–^{13}C HMQC experiment was recorded, at natural abundance ^{13}C. Indeed, the corresponding ^{13}C–^{1}H signals were observed at 88 ppm in a region of C1' (83–89 ppm) apart from the C3' resonances (75–81 ppm). The ^{13}C resonance position as well as the $^1J(^{13}C–^{1}H) coupling constant (183 Hz) is in the range expected for a ^{13}C1'–H1' cross peak. That the H1' resonance is not mixed up with an H3' resonance is also obvious from the ^{1}H–^{31}P HMQC spectrum. In Figure 4 part of the NOESY spectrum and the corresponding ^{1}H–^{31}P HMQC spectrum are shown. The cross peaks between H2' and H2'' on the one hand and H1', H3', and H4' of the same residue on the other hand are connected by lines. ^{1}H–^{31}P cross peaks involving H3' and H4' are observed in the HMQC spectrum, but not between the H1' and any phosphorous. After unequivocally demonstrating the correctness of the assignment of the upfield-shifted (L)T$_4$H1' resonance, we return to the cross peaks depicted in Figure 3 where we can now complete the sequential analysis since connectivities are found between T$_4$H1' and T$_4$H6 as well as T$_4$H1' and G$_5$H8 resonances. Note that there are minor differences in the chemical shifts between Table 2 and Figure 3, due to minor differences in temperature. This spectrum was chosen for Figure 3 since the particular cross peak which connects T$_4$H1' and G$_5$H8 is observed at this mixing time. Finally, the

assignment of the other sugar resonances is achieved by means of the TOCSY spectrum in combination with the ^{1}H–^{31}P HMQC spectrum. The assignments are collected in Table 2.

The resonances of the backbone protons in the central portion of the duplex, i.e., around the L-nucleoside, are particularly important, and a part of the NOESY spectrum recorded with a mixing time of 200 ms and the corresponding ^{1}H–^{31}P HMQC spectrum are presented in Figure 4. In Figure 4 the connectivities are drawn which connect the backbone protons and phosphorous atoms in the inserted schematic structure. The cross peaks of the H2′–H3′ and H2″–H3′ proton pairs of G_3 can readily be found in the NOESY spectrum. Then, the phosphorous resonance P_4 is found in the ^{1}H–^{31}P HMQC spectrum at 1.4 ppm. P_4 also exhibits cross peaks to the backbone protons of (L)T_4. The magnetization is transferred from P_4 not only to H5′ and H5″ but also to the H4′ resonance, indicating that the $^4J_{PH4'}$ coupling is not equal to zero. The latter indicates that the lines connecting the atoms in the sequence P–O5′–C5′–C4′–H4′ are found in a planar W-shaped conformation. This feature only occurs when γ adopts a gauche($+$) conformation and β simultaneously adopts a trans conformation. The H5′ and H5″ proton resonances were assigned stereospecifically by comparing the corresponding intensities of the H5′–H3′ and H5″–H3′ cross peaks in the NOESY spectrum (Blommers et al., 1991). The H4′ resonance can be connected to the H3′ resonance of T4 in the 2D spectrum in the top panel of Figure 4. Subsequently, P_5 is found as well as the backbone proton resonances of G5. Most of the ^{31}P resonances fall in a narrow region around 0.4 ppm. The resonances of P_4 and P_5 as well as the resonance of the phosphorous between C_{10} and A_{11} (H3′ as well as ^{31}P resonances are overlapping for C_{12} and T_4) are shifted downfield. This may indicate that one of the torsion angles α or ζ adopts a trans conformation instead of the gauche($-$) conformation normally observed for natural oligonucleotides.

(C) Analysis of the Conformation of the Deoxyribose Units. NMR studies of short oligonucleotides have demonstrated that the sugar ring is not rigid (Van de Ven & Hilbers, 1988a). The experimentally obtained vicinal *J*-couplings, describing the sugar conformation, have satisfactorily been described by assuming an equilibrium between an N-type and an S-type conformation (Altona, 1982). For larger oligonucleotides, *J*-coupling constants are generally extracted from 2D spectra, rather than from 1D spectra, and are for this reason less accurate. For the present investigation all sums of *J*-couplings were determined from the DQF-COSY spectrum. In principle, the sums represent the same information as the individual coupling constants. These data were used as input for the program MARC, which scans through a database of calculated coupling constants. It was found that all sugars adopt predominantly an S-type conformation. Results are collected in Table 3. Because no assumption was made about the conformation, our analysis demonstrates that the experimental data would be in conflict with any sugar conformation in case a rigid sugar is assumed. This is the case for G_1, G_7, C_{12}, and G_{13}. It is not surprising that the terminal residues G_1 and G_7 are more flexible. In the case of C_{12} there is enough experimental evidence to believe that the sugar motion differs from the others, i.e., roughly 78% S-type/22% N-type. This observation is interesting since this sugar ring is part of the G_3·C_{12} base pair, which is the 5′ neighbor base pair of the unnatural (L)T_4·A_{11} pair. One would expect changes in the conformation or dynamics of the L-sugar; instead, the analysis shows that this is not the case. The L-sugar adopts predominantly an S-type conformation. As we can read from Table

Table 3: Results of the Conformational Analysis of the Mononucleotide Building Blocks of d(G_1-C_2-G_3-(L)T_4-G_5-C_6-G_7)·d(C_8-G_9-C_{10}-A_{11}-C_{12}-G_{13}-C_{14}) (Duplex II)^a

res	$\Sigma 1'$	$\Sigma 2'$	$\Sigma 2''$	$x(S)$	χ
G_1	14.8	25.4	23.0	0.65–0.90	170–280
C_2	14.8	29.7	21.2	0.80–1.00	170–280
G_3	15.3			0.70–1.00	238–244
T_4	15.7	29.2		0.85–1.00	150–183
G_5	15.7	26.6		0.65–1.00	240–245
C_6	14.8	29.7	21.2	0.85–1.00	230–240
G_7	14.8	27.2	21.8	0.90–0.95	170–280
C_8	14.8	28.5	21.9	0.80–1.00	218–220
G_9	15.7			0.80–1.00	170–280
C_{10}	15.7	28.0	19.8	0.90–1.00	242–250
A_{11}	16.0			0.90–1.00	244–254
C_{12}	14.8	29.5	23.3	0.70–0.85	210–240
G_{13}		26.6		0.15–0.95	228–238
C_{14}	14.3			0.50–1.00	170–280

^{a} The conformation of all sugars is S-type. The population of the S-conformation, $x(S)$, could be derived from the sums of the coupling constants measured from the DQF-COSY spectrum in conjunction with the program MARC. The conformations of the base relative to the sugar, χ, were established from relaxation matrix calculations using the program NOESIM and the NOE intensities of the 500-MHz NOESY spectrum, recorded with a mixing time of 200 ms.

3, the *J*-coupling data available for the L-sugar are consistent assuming one sugar conformation.

(D) Determination of the Glycosidic Torsion Angle. The glycosidic torsion angle has been determined using the experimentally obtained NOE intensities observed for the H6/8–H1′/H2′/H2″/H3′ pairs of the NOE spectrum, recorded with a mixing time of 200 ms. The intensities were scaled using the average intensity of the NOEs corresponding to the cytidine H5–H6 resonances. Only those NOEs which do not overlap with other signals were used. The intensities were calculated as a function of the sugar conformation and glycosidic torsion angles using relaxation matrix calculations, assuming a rotational correlation time of 1.5 ns. Results of the analysis are collected in Table 3. Apart from the L-nucleoside, all glycosidic torsion angles are in the range normally observed for a B-type double-helical structure. The orientation of the base in the L-nucleoside is anti, but the glycosidic torsion angle in this residue falls outside of the range normally observed (cf. Table 3).

(E) Determination of Interresidual Distances. The conformations of the mononucleotide building blocks suggest that the conformation of both ends of the duplex, involving the C·G pairs, is close to that of a B-type helix. Further analysis of the interresidual NOEs as well as the coupling constants describing the backbone torsion angles, when available, support this assumption. The geometrical information which can be extracted from the present experimental data is not sufficient for an accurate structure determination of this less interesting part of the duplex. For the moment, a B-type helix is assumed, and we will focus our attention to elucidate a detailed structure of the central part of the duplex around the (L)T·A base pair.

An analysis of NOESY spectra recorded at 200- and 400-ms mixing times resulted in the detection of numerous contacts between these protons in the central part of the duplex. The connectivities between protons in adjacent residues are summarized in Figure 5. Eight contacts were found between the residues G_3 and (L)T_4. These involve contacts between the aromatic and methyl protons and the protons of the 5′ neighbor residue. In addition, NOEs were observed between the H1′ resonance of G_3 and the H2′ and H2″ resonances of (L)T_4. These cross peaks could be assigned unambiguously
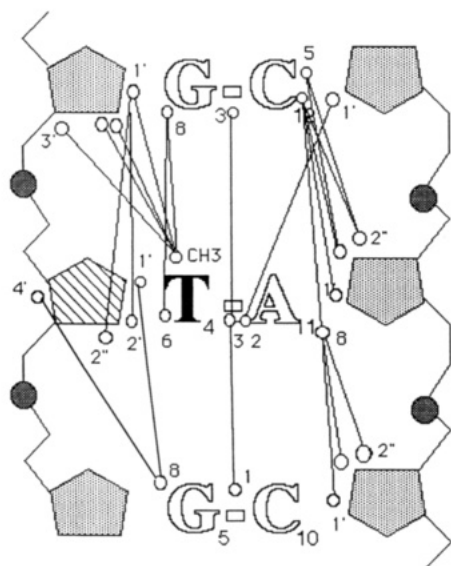
FIGURE 5: Summary of the NOEs observed between the proton resonances in the central part of duplex **II**.

by comparison of the NOESY with the DQF-COSY and TOCSY spectra. The two NOE cross peaks fall in an empty region in the latter two spectra. Also, connectivities are found between residue G$_5$ and (L)T$_4$. The connectivities observed between residues C$_{10}$ and A$_{11}$ in the complementary strand are those which one would expect for regular DNA; i.e., cross peaks were found between the aromatic proton resonance of A$_{11}$ and its 5'-neighbor sugar proton resonances. These cross peaks are also observed for the A$_{11}$-C$_{12}$ step, but in addition interresidue cross peaks are observed involving the H5 resonance of C$_{12}$. These connectivities are predicted for B-DNA, but when one inspects the cross-peak intensities, one finds that the interresidue cross peak H6–H1' is stronger in intensity than the cross peak H8–H2'', which is an indication that this step deviates from the B-type helix (Haasnoot et al., 1984).

Using the NOE intensities and the conformations of the mononucleotide building blocks (vide supra) as input for the program NOEFIT, the calculated relaxation matrix is fitted by a sequential determination of the interresidue distances. Results obtained for a mixing time of 200 ms are collected in Table 4. Similar results were obtained using the NOE intensities obtained with other mixing times.

(F) Determination of Backbone Torsion Angles. The structure of the sugar–phosphate backbone is described by the six torsion angles α–ζ. A crucial element in the structure elucidation of nucleic acids is the determination of these torsion angles, by studying homo- and heteronuclear coupling constants. To this end, the backbone torsion angles have been determined in a qualitative approach as described earlier (Blommers et al., 1991); i.e., on the basis of the experimental data, the torsion angles are assigned to the gauche(+), trans, or gauche(–) region for the dominant rotamer.

The estimation of the torsion angle γ follows after an analysis of NOEs between aromatic resonances and H5'/H5'' resonances and $J_{4'5'}$ and $J_{4'5''}$ coupling constants, when available, from the DQF-COSY spectrum. Since neither a coupling constant on the order of 10 Hz nor any medium strong NOEs were observed in the above mentioned region, it is concluded that the torsion angle γ adopts the gauche(+) conformation for all D-sugars and the gauche(–) one for (L)T$_4$.

The torsion angle β usually adopts a trans conformation, and consequently small $J_{5'P}$ and $J_{5''P}$ heteronuclear coupling

Table 4: Distance Restraints Used As Input for Distance-Geometry Calculations of Duplex II[a]

proton	proton	NOE	lower bound	upper bound
G3H1'	T4H2'	0.019	2.85	3.96
G3H1'	T4H2''	0.007	3.95	5.49
G3H2'	T4CH3	0.008	3.35	4.65
G3H2''	T4CH3	0.008	3.49	4.85
G3H3'	T4CH3	0.002	4.68	6.50
G3H8	T4CH3	0.012	3.30	4.59
G3H8	T4H6	0.005	3.83	5.31
G3H1	T4H3	0.094	1.80	4.00
G3H4'	T4CH3	0.000	4.00	∞
G3H1'	T4CH3	0.000	4.00	∞
G3H1'	T4H1'	0.000	4.00	∞
G3H1'	T4H2'	0.000	4.00	∞
G3H1'	T4H2''	0.000	4.00	∞
G3H1'	T4H6	0.000	4.00	∞
G3H1'	A11H2	0.000	4.00	∞
G3H2'	T4H1'	0.000	4.00	∞
G3H2'	T4H2'	0.000	4.00	∞
G3H2'	T4H5'	0.000	4.00	∞
G3H2'	T4H5''	0.000	4.00	∞
G3H2''	T4H1'	0.000	4.00	∞
G3H2''	T4H2'	0.000	4.00	∞
G3H2''	T4H5'	0.000	4.00	∞
G3H2''	T4H5''	0.000	4.00	∞
G3H3'	T4H1'	0.000	4.00	∞
G3H4'	T4H1'	0.000	4.00	∞
G3H8	T4H2'	0.000	4.00	∞
G3H8	T4H5'	0.000	4.00	∞
G3H8	T4H5''	0.000	4.00	∞
T4H1'	G5H8	0.007	3.62	5.03
T4H4'	G5H8	0.008	3.56	4.95
T4H3	A11H2	0.115	1.80	4.00
T4H3	G5H1	0.094	1.80	4.00
T4CH3	G5H8	0.000	4.00	∞
T4CH3	G5H1'	0.000	4.00	∞
T4CH3	G5H2'	0.000	4.00	∞
T4CH3	G5H2''	0.000	4.00	∞
T4H1'	G5H2'	0.000	4.00	∞
T4H1'	A11H2	0.000	4.00	∞
T4H2'	G5H8	0.000	4.00	∞
T4H2''	G5H8	0.000	4.00	∞
T4H6	G5H8	0.000	4.00	∞
T4H4'	G5H2'	0.000	4.00	∞
T4H4'	G5H2''	0.000	4.00	∞
T4H2'	G5H5'	0.000	4.00	∞
T4H2'	G5H5''	0.000	4.00	∞
T4H2''	G5H5''	0.000	4.00	∞
G5H1'	A11H2	0.000	4.00	∞
C10H1'	A11H8	0.012	3.22	4.48
C10H2'	A11H8	0.004	4.32	6.00
C10H2''	A11H8	0.007	3.54	4.91
C10H6	A11H2	0.000	4.00	∞
C10H5	A11H1'	0.000	4.00	∞
A11H1'	C12H6	0.011	3.35	4.65
A11H1'	C12H4'	0.005	3.90	5.41
A11H2'	C12H6	0.014	3.06	4.25
A11H2'	C12H5	0.014	3.09	4.29
A11H2''	C12H6	0.001	4.10	6.25
A11H2''	C12H5	0.001	4.10	6.25
A11H2	A11H1'	0.001	4.10	6.25
A11H8	C12H6	0.003	4.46	6.20
A11H2	C12H6	0.000	4.00	∞
A11H1'	C12H1'	0.000	4.00	∞
A11H1'	C12H2'	0.000	4.00	∞
A11H1'	C12H2''	0.000	4.00	∞
A11H1'	C12H3'	0.000	4.00	∞
A11H1'	C12H5	0.000	4.00	∞
A11H3'	C12H6	0.000	4.00	∞

[a] The distances were obtained using measured interresidual NOE intensities of the 500-MHz NOESY (mixing time 200 ms) and the conformations of the mononucleotide building blocks (cf. Table III). These were used as input for the program NOEFIT, which fits the interresidue distances using a relaxation matrix approach. The distances were translated into upper and lower bounds by adding 25% and subtracting 10% from these distances. The average NOE intensity of the H5–H6 cross peaks of cytosine is 0.104. A value of 1.5 ns is chosen for the rotational correlation time. Also a number of unobserved NOEs are indicated. For these non-NOEs no signal is found for NOESY spectra with mixing times up to 500 ms. For the NOEs found for exchangeable protons the upper bound is set to 4 Å.

constants are observed. For the gauche(+) and gauche(−) conformations one expects to observe one large heteronuclear coupling constant on the order of 23 Hz. Such a coupling constant is not observed in either the homonuclear spectra or the ^{1}H–^{31}P HMQC, where the heteronuclear coupling constant is observed as the active coupling. It is therefore concluded that all β torsion angles in this duplex adopt a trans conformation. The combination γ^-/β^t for the L-residue and γ^+/β^t for some D-residues is confirmed in some favorable cases in the HMQC spectrum by the observation of magnetization transfer between P and H4′ through four bonds.

The torsion angles α and ζ around the phosphorus adopt the α^-/ζ^- conformation in the regular A- and B-type helices. When α or ζ switches to the trans conformation, the phosphate resonance shifts downfield. This is observed for the P_4 and P_5 resonances of the phosphorus atoms which connect the L-nucleoside to the two D-strands (cf. Figure 4), as well as for the resonance of the phosphorus connecting C_{12} and G_{13} in the natural opposite strand. These resonances shift 0.6–1.0 ppm downfield from the bulk of ^{31}P resonances. This indicates that in these three cases the conformation around the phosphates may be different from α^-/ζ^-.

The torsion angle ϵ has been determined using $^3J_{HP}$ and $^4J_{HP}$ coupling constants. The gauche(+) conformation, for which it is claimed that this conformation is forbidden (Altona, 1982), is connected to a $J_{H3'P}$ coupling constant around 23 Hz. Such a large coupling constant, as either active or passive coupling, is not observed in any of our 2D spectra. The discrimination between the ϵ^- and ϵ^t conformations can be achieved using the four-bond coupling constant $J_{H2'P}$ (Blommers et al., 1991). In our molecule all the sugars predominantly adopt an S-type conformation. Then, when ϵ adopts a gauche(−) conformation, the bonds between H2′ and P form a flat W. Thus, in an ϵ^- conformation we have the situation that not only are the H2′ and H3′ resonances coupled, but both spins are also coupled to the same heteronucleus (^{31}P). Since the ^{31}P nucleus is not pulsed during the DQF-COSY experiment, one would expect for the ϵ^- case E-COSY-type cross peaks for the H2′–H3′ resonances (M. J. J. Blommers and O. Zerbe, unpublished results). No E-COSY-type cross peaks are observed for the H2′–H3′ resonances; thus, ϵ adopts a trans conformation in all D-residues and in the L-nucleoside as well.

Finally, the value of δ is intimately connected to the sugar conformation, which is in all cases S-type (which results in a trans conformation of δ).

Interestingly, the incorporation of the mirror image sugar has been achieved by rotations involving only the glycosidic torsion angle and the torsion angles α/ζ around the phosphates connecting the L-nucleoside. All other torsion angles are as in a regular helix. The complementary strand also accommodates itself by changing just one of the phosphate backbone angles.

(G) Structure Calculation. The examination of the experimental data as described in the previous sections has resulted in a collection of geometrical information regarding the structure of the duplex formed between d(G-C-G-(L)T-G-C-G) and d(C-G-C-A-C-G-C) in solution. This information was subsequently converted into a suitable input for distance geometry calculations. Table 4 gives the list of distance restraints used. Since non-NOEs provide useful additional restraints, a set of unambiguous lower bound restraints was collected for those cases where no NOE cross peak appeared in NOESY spectra up to 500 ms. In addition, torsion angle restraints were set for the endocyclic torsion

angles of the sugar as well as for the glycosidic torsion angles derived from the relaxation matrix calculations. The backbone torsion angles γ, β, and ϵ were defined using upper and lower bounds which vary 15° around the rotamers usually found; i.e. γ^+ is 38–68° (Haasnoot, 1981), β^t is 181–211°, and ϵ^t is 177–207° (Lankhorst, 1984). The torsion angles α and ζ were not restrained. Only at both ends of the duplex, where the collection of a sufficient number of restraints is hampered by overlap of cross peaks, are distances obtained from a B-type helix used. Using these restraints as input for the program DGII, a set of 20 structures was calculated by distance geometry followed by simulated annealing. From these calculations it was evident that the thymidine NH proton is close enough to the adenine N1 and that the amino protons of adenine are close enough to the thymidine oxygen to permit hydrogen bond formation. The distance between the pairs of atoms involved varies between 2.0 and 2.5 Å. It is concluded that $(L)T_4$ and A_{11} form a Watson–Crick type base pair. Since no other alternative base pair is apparent from the distance geometry structures, the hydrogen bonds were added to the restraint list and distance geometry and simulated annealing were repeated for 200 structures.

Figure 6 shows a representative structure of the duplex. A superposition of a number of structures of the central part of the duplex is given in Figure 7. All structures satisfy the distance restraints. Some of the structures violate the torsion bounds. However, all torsion angles satisfy the gauche(+), trans, or gauche(−) domains corresponding to the observations by NMR.

Clearly the DNA molecule adopts a B-type structure, with a slight change of the helical axis around the (L)T·A base pair, which is of the Watson–Crick type (vide infra). The region comprising base pairs G_3·C_{12} and $(L)T_4$·A_{11} is especially well defined by the NMR data (cf. Figure 7).

The structure has been further probed by molecular mechanics and dynamics calculations: e.g., one of the distance geometry structures was subjected to an energy minimization and a molecular dynamics simulation over 100 ps without the experimental constraints. All structural aspects were conserved during the simulation.

DISCUSSION AND CONCLUSION

The NMR studies presented in this paper demonstrate that it is possible, without major adjustments, to replace a D-sugar for a L-sugar in a duplex with natural chirality. The changes required for such an arrangement are observed in the torsion angles α and ζ; i.e., one of these torsion angles changes to a trans conformation. The structure of the G_3-$(L)T_4$-G_5 segment is given by the following backbone torsion angles: $[G_3]$–ϵ^t–$(\zeta^-$–α^t/ζ^t–$\alpha^+)$–β^t–γ^-–$[(L)T_4]$–ϵ^t–$(\zeta^+$–α^t/ζ^t–$\alpha^-)$–β^t–γ^+–$[G_5]$. This change is observed around the phosphates which connect the L-residue to the neighboring D-residues on the same strand as well as in the same region of the paired natural strand. The $\alpha^t\zeta^t$ rotamers, which are also found in the distance geometry calculations, should be neglected, since they have high energies (Platt et al., 1981). It is noted that the observation of α^t and ζ^t rotamers in the distance geometry structures finds its experimental confirmation in the observed chemical shifts of the phosphorus nuclei; i.e., the three phosphate resonances shift around 1 ppm downfield from the bulk of resonances. Chemical shift considerations were not used as input for the distance geometry calculations.

All other backbone torsion angles remain in the range observed for right handed helices, i.e., $\alpha^-\beta^t\gamma^+\delta^t\epsilon^t\zeta^-$. The backbone torsion angles in the L-residue are correspondingly
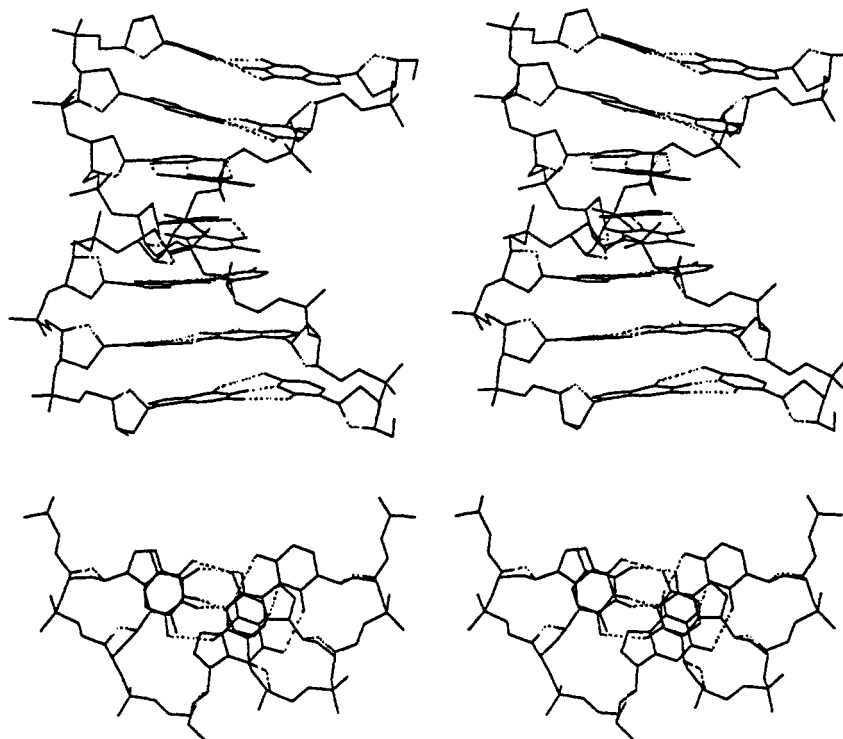
FIGURE 6: Structure of duplex II in stereo view. The nonexchangeable protons are not shown. The hydrogen bonds and the bonds to the sugar O4' atoms are represented by dashed lines. Panel A, top, represents the duplex perpendicular to the helix axis. Panel B, bottom, is a view along the helix axis of the central three base pairs. The L-thymidine is found in the left strand.

FIGURE 7: Superposition of a representative number of distance geometry structures of duplex II. The (L)T$_4$·A$_{11}$/G$_3$·C$_{12}$ base step is shown. Only atoms of this part of the structure are superimposed. The figure demonstrates the good quality of the NMR structure, which was determined by experimental restraints only.

$\beta'\gamma^-\delta'\epsilon'$. All sugar residues adopt predominantly an S-type conformation. The sugar of residue C$_{12}$, which is next to A$_{11}$ and which pairs to L(T$_4$), is, apart from terminal residues, more flexible than the others. Here, roughly 22% N-type conformations are observed. It is noted that a transition between the S- and N-type conformations of C$_{12}$ is observed during the molecular dynamics calculations. Thus, the local geometry in our structure allows the sugar to convert from S- to N-type, rather easily. Finally, the incorporation of the L-sugar goes concomitantly with a change of the glycosidic torsion angle χ in the L-sugar to a value close to 180°.

In conclusion, changes in α, ζ and χ allow the incorporation of a L-residue without changing the overall geometry of the duplex, e.g. position and type of the base pairs, position of the phosphates.

An independent, more qualitative NMR study of the self-complementary oligonucleotide d(C-G-C-(L)G-A-A-T-T-C-G-C-G) suggests that the (L)G is involved in a stable Watson–Crick C·G pair (Urata et al., 1993). The two NOEs observed between the residues in the C-(L)G-A region of the duplex are also observed in the present study. The conformation

of the (L)G residue is similar to that of (L)T in the present study (Blommers et al., 1993).

While L-DNAs do not form, in general, stable duplexes with D-DNA or D-RNA, this study demonstrates that it is possible to incorporate a L-sugar within a natural strand and retain the classical base-pairing scheme. The thermodynamic properties of heterochiral duplexes depend on the sequence and/or the type of the L-nucleoside. This conclusion is also evident from the work of Damha and co-workers (Damha et al., 1994). UV melting experiments have shown that duplex II is more stable than duplex III. For example, the thymidine NH proton in duplex III is more accessible to the solvent than the thymidine NH in duplex II. There are two factors which explain this difference in stability: (1) The angles T$_4$N1–T$_4$C1'–A$_{11}$C1' and T$_4$C1'–A$_{11}$C1'–A$_{11}$N9 are 57° and 53°, respectively. These angles are almost equal for Watson–Crick pairs in a standard duplex, and for this reason, the A·T and C·G pairs can readily be inverted; i.e., the base pairs have a pseudoaxis of symmetry. This pseudoaxis of symmetry is obviously not present in the (L)T·A base pair. Thus, when (L)T·A is replaced by T·(L)A, the formation of a base pair requires changes in the structure. Indeed, preliminary data of duplex III suggest changes in the backbone torsion angles relative to duplex II. (2) The overlap of six-membered rings observed for the G$_3$-(L)T$_4$ /A$_{11}$-C$_{12}$ part of the molecule (cf. Figure 6B and Figure 8) is not conserved when purines are replaced by pyrimidines and vice versa. Thus, this type of interaction may most likely be found only for (D)Pu-(L)Py sequences.

The thermodynamic properties of the duplexes listed in Table 1 differ substantially. Because one may expect the enthalpy of the *random-coil* single-stranded sequences to be almost equal, the substitution of the one L-thymidine for D-thymidine in duplex II results in a significant stabilization in enthalpy. The value found for $\Delta\Delta H$, 14 kcal, is on the order of the formation of an extra C·G base pair. However,
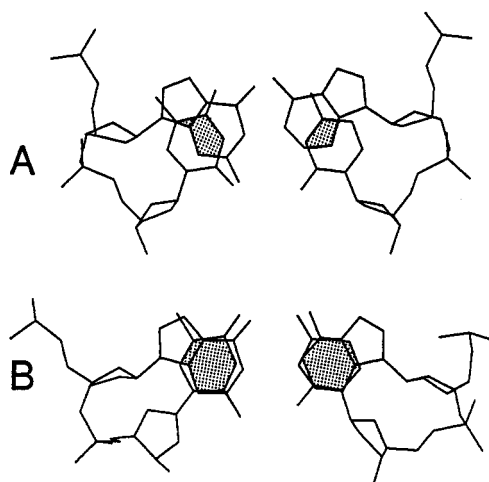
FIGURE 8: Comparison between the base overlaps in the $T_4 \cdot A_{11}/G_3 \cdot C_{12}$ base pair step in B-DNA and the $(L)T_4 \cdot A_{11}/G_3 \cdot C_{12}$ base pair step observed in the experimental structure of duplex II. The structure is viewed in the same orientation as in Figure 7. The nonexchangeable protons are omitted. The overlap of the six-membered aromatic rings in panel B suggests interactions between the π orbitals of the aromatic rings.

the effect on the enthalpy does not result in a dramatic change in free energy, since the system also loses entropy (cf. Table 1). Since the difference in enthaply clearly exceeds the accuracy of the thermodynamic data, the observed effects should be considered as significant. The structure found experimentally for d(G-C-G-(L)T-G-C-G)·d(C-G-C-A-C-G-C) provides a plausible explanation of the difference in enthalpy and entropy. The structure of the base step G_3-T_4/A_{11}-C_{12} is well defined by the NMR data and results in a locally accurate structure (cf. Figure 7). Further examination of this part of the duplex shows that the six-membered rings which are part of the purines have an almost ideal overlap with the six-membered rings of the pyrimidines, allowing the π orbitals of both systems to interact strongly. Such an interaction clearly differs from the normal base–base stacking observed in nucleic acids. This is illustrated in Figure 8, where the overlap of the six-membered rings observed in duplex II is compared with a standard B-type DNA molecule with the same base composition. The interaction between the orbitals is then most likely connected with a very deep and narrow energy minimum, which explains the low enthalpy (deep) and the low entropy (narrow). Other effects which influence the entropy may be found in the packing of the L-sugar in the duplex. The space between the sugar residues of G_3 and $(L)T_4$ is completely filled with the van der Waals spheres of the sugar protons, which indicates good hydrophobic interactions as well as rigidity in this part of the structure.

The interaction between the π orbitals as suggested in the previous lines has not, to our knowledge, been noted before. However, the overlap is preserved during the molecular dynamics simulations which have been carried out after the discovery of this feature by distance geometry calculations. The observed interactions can therefore be considered consistent with the AMBER force field. The unusual chemical shifts, e.g., T_4H1', $C_{10}H1'$, and T_4NH, may be due to the unusual electronic environments of these protons.

One of the prerequisites in the design of candidate antisense oligonucleotides, i.e., oligonucleotides that are resistant to nucleases and that form selective and stable hybrids with DNA or RNA, is the understanding of the interactions in these unnatural systems. To this end, detailed structural studies of model systems, like the one presented here, give information

which may prove expedient to the development of valuable antisense tools.

REFERENCES

Altona, C. (1982) *Recl. Trav. Chim. Pays-Bas 101*, 413–433.

Asseline, U., Hau, J.-F., Czernecki, S., Le Diguarher, T., Perlat, M.-C., Valery, J.-M., & Thuong, N. T. (1991) *Nucl. Acids Res. 19*, 4067–4074.

Barkhuijsen, H., de Beer, R., Bovee, W. M. M. J., & van Ormondt, D. (1985) *J. Magn. Reson. 61*, 465–481.

Blommers, M. J. J., Haasnoot, C. A. G., Hilbers, C. W., van Boom, J. H., & van der Marel, G. A. (1987) Structure and dynamics of biopolymers, *NATO ASI Ser., Ser. E 113*, 78–91.

Blommers, M. J. J., van de Ven, F. J. M., van der Marel, G. A., van Boom, J. H., & Hilbers, C. W. (1991) *Eur. J. Biochem. 201*, 33–51.

Blommers, M. J. J., Capobianco, M. L., Colonna, F. P., Tondelli, L., & Garbesi, A. (1993) *J. Mol. Graphics 11*, 264.

Braunschweiler, L., & Ernst, R. R. (1983) *J. Magn. Reson. 53*, 521–558.

Capobianco, M. L., Garbesi, A., Arcamone, F., Maschera, B., & Palu, G. (1991) *Nucleic Acids Symp. Ser. 24*, 274.

Damha, M. J., Giannaris, P. A., Marfey, P., & Reid, L. S. (1991) *Tetrahedron Lett. 32*, 2573–2576.

Damha, M. J., Giannaris, P. A., & Marfey, P. (1994) Biochemistry (preceding paper in this issue).

Editors (1993) *Antisense Res. Dev. 3*, 95–153.

Egholm, M., Buchardt, O., Christensen, L., Beherens, C., Freier, S. M., Driver, D. A., Berg, R. H., Kim, S. H., Norden, B., & Nielsen, P. E. (1993) *Nature 365*, 566–568.

Freier, S. M., Kierzek, R., Jaeger, J. A., Sugimoto, N., Carothers, M. H., Neilson, T., & Turner, D. (1986) *Proc. Natl. Acad. Sci. U.S.A. 83*, 9373–9377.

Fritsch, V., & Westhof, E. (1990) Modelling of Molecular Structures and Properties, *Stud. Phys. Theor. Chem. 71*, 627–634.

Garbesi, A., Capobianco, M. L., Colonna, F. P., Tondelli, L., Arcamone, F., Manzini, G., Hilbers, C. W., Aelen, J. M. E., & Blommers, M. J. J. (1993) *Nucleic Acids Res. 21*, 4159–4165.

Gralla, J., & Crothers, D. M. (1973) *J. Mol. Biol. 73*, 497–511.

Griesinger, C., Otting, G., Wüthrich, K., & Ernst, R. R. (1988) *J. Am. Chem. Soc. 110*, 7870–7872.

Haasnoot, C. A. G., & Hilbers, C. W. (1983) *Biopolymers 22*, 1259–1266.

Haasnoot, C. A. G., Westerink, H. P., van der Marel, G. A., & van Boom, J. H. (1983) *J. Biomol. Struct. Dyn. 1*, 131–149.

Haasnoot, C. A. G., Westerink, H. P., Van der Marel, G. A., & Van Boom, J. H. (1984) *J. Biomol. Struct. Dyn. 2*, 345–360.

Hare, D. R., Wemmer, D. E., Chou, S.-H., Drobny, G., & Reid, B. R. (1983) *J. Mol. Biol. 171*, 319–336.

Havel, T. F. (1991) *Prog. Biophys. Mol. Biol. 56*, 43–78.

Hélène, C., & Toulme, J.-J. (1990) *Biochim. Biophys. Acta 1049*, 99–125.

Imbach, J.-L., Rayner, B., & Morvan, F. (1989) *Nucleosides Nucleotides 8*, 627–648.

Jeener, J., Meier, B. H., Bachmann, P., & Ernst, R. R. (1979) *J. Chem. Phys. 71*, 4546–4553.

Keepers, J. W., & James, T. L. (1984) *J. Magn. Reson. 57*, 404–426.

Lankhorst, P. P. (1984) Carbon-13 and proton NMR studies of RNA and DNA constituents, Thesis, Leiden, The Netherlands.

Marshall, W. S., & Caruthers, M. H. (1993) *Science 259*, 1564–1570.

Milligan, J. F., Matteucci, M. D., & Martin, J. C. (1993) *J. Med. Chem. 36*, 1923–1937.

Morvan, F., Porunb, H., Degols, G., Lefevre, I., Pompom, A., Sproat, B. S., Rayner, B., Malvy, C., Lebleu, B., & Imbach, J.-L. (1993) *J. Med. Chem. 36*, 280–287.

Piantini, U., Sorenson, O. W., & Ernst, R. R. (1982) *J. Am. Chem. Soc. 104*, 6800–6801.

Platt, E., Robson, B., & Hillier, I. H. (1981) *J. Theor. Biol. 88*, 333–353.

Spadari, S., Maga, G., Focher, F., Ciarrocchi, G., Manservigi, R., Arcamone, F., Capobianco, M., Carcuro, A., Colonna, F., Iotti, S., & Garbesi, A. (1992) *J. Med. Chem. 35*, 4214–4220.

States, D. J., Haberkorn, R. A., & Ruben, D. J. (1982) *J. Magn. Reson. 48*, 286.

Thuong, N. T., & Hélène, C. (1993) *Angew. Chem., Int. Ed. Engl. 32*, 666–690.

Uhlmann, E., & Peyman, A. (1990) *Chem. Rev. 90*, 543–584.

Urata, H., Ueda, Y., Suhara, H., Nishioka, E., & Akagi, M. (1993) *J. Am. Chem. Soc. 115*, 9852–9853.

Van de Ven, F. J. M., & Hilbers, C. W. (1988a) *Eur. J. Biochem. 178*, 1–38.

Van de Ven, F. J. M., & Hilbers, C. W. (1988b) *Nucleic Acids Res. 16*, 5713–5723.

Van de Ven, F. J. M., Blommers, M. J. J., Schouten, R. E., & Hilbers, C. W. (1991) *J. Magn. Reson. 94*, 140–151.

Weiner, S. J., Kollman, P. A., Ngygen, D. T., & Case, D. A. (1986) *J. Comput. Chem. 7*, 230–235.

Yaswen, P., Stamper, M. R., Ghosh, K., & Cohen, J. S. (1993) *Antisense Res. Dev. 3*, 67–77.